Photoconductive Cadmium Sulfide Hemicylindrical Shell Nanowire Ensembles

ARTICLE *in* NANO LETTERS · OCTOBER 2005

Impact Factor: 13.59 · DOI: 10.1021/nl050994x · Source: PubMed

NANO LETTERS

2005
Vol. 5, No. 9
1720−1725

Photoconductive Cadmium Sulfide Hemicylindrical Shell Nanowire Ensembles

Qiguang Li and Reginald M. Penner*

Department of Chemistry, University of California, Irvine, California 92697-2025

Received May 27, 2005; Revised Manuscript Received July 20, 2005

ABSTRACT

We report the synthesis and characterization of hemicylindrical shell nanowires (HSNWs) composed of nanocrystalline cadmium sulfide (CdS). CdS HSNWs were synthesized by first electrodepositing microcrystalline cadmium (Cd) nanowires by electrochemical step-edge decoration on graphite electrode surfaces and then converting these Cd nanowires into CdS by exposure to H_2S at elevated temperature. These nanowires had a hemicylindrical shell morphology that was produced by the Kirkendall effect, involving disparate rates for diffusion of Cd and S atoms within the nascent CdS layer during the conversion from Cd to CdS. The outer diameter of the CdS HSNWs was 1.6–2.4 times that of Cd precursor nanowires and was adjustable over the range from 116 to 550 nm. CdS HSNWs showed strong, band-edge photoluminescence at 2.45 eV and a fast, reversible, and stable photoconductivity response in air characterized by "on" and "off" times of less than 15 ms.

Nanowires composed of direct-gap semiconductors have the potential to function as transistors in which light gates the flow of charge from one end of the nanowire to the other. In such devices, light with energy greater than the band gap is absorbed by the nanowire producing mobile electrons and holes that increase the conductivity of the nanowire. The photoconductivity performance of the nanowires investigated to date, however, has revealed an unexpected limitation: the conductivity of photoexcited nanowires requires between seconds and minutes to decay in the dark. In the case of single-crystalline ZnO nanowires, dark photoconductivity decays of 50−15 000 s (~4 h) have been attributed to slow surface oxygen photochemistry coupled with a surface space charge.[1−9] Slow photocurrent decays with time constants of 1−1000 s have also been reported for nanowires composed of GaN,[10] SnO_2,[2,9] and In_2O_3,[11] but the reasons for these slow photoconductivity dark decays are unclear. We are unaware of published photoconductivity responses faster than those reported in these papers.

Here we describe the synthesis of nanocrystalline CdS hemicylindrical shell nanowires (HSNWs) that are between 116 and 550 nm in diameter and electrically continuous for lengths of up to 1 mm. Previously, a variety of different CdS nanostructures have been synthesized including quantum dots,[12,13] nanorods,[14] nanowires,[15] nanobelts,[16] and nanoribbons.[17] The two-step electrochemical/chemical (E/C) method[12,18,19] employed here for obtaining CdS HSNW arrays (Scheme 1) involves the preparation of cadmium (Cd) nanowires by electrochemical step-edge decoration (ESED) on HOPG electrodes in the first step, according to the reaction

Scheme 1. E/C Method for Synthesizing CdS Hemicylindrical Shell Nanowires on Graphite Surfaces

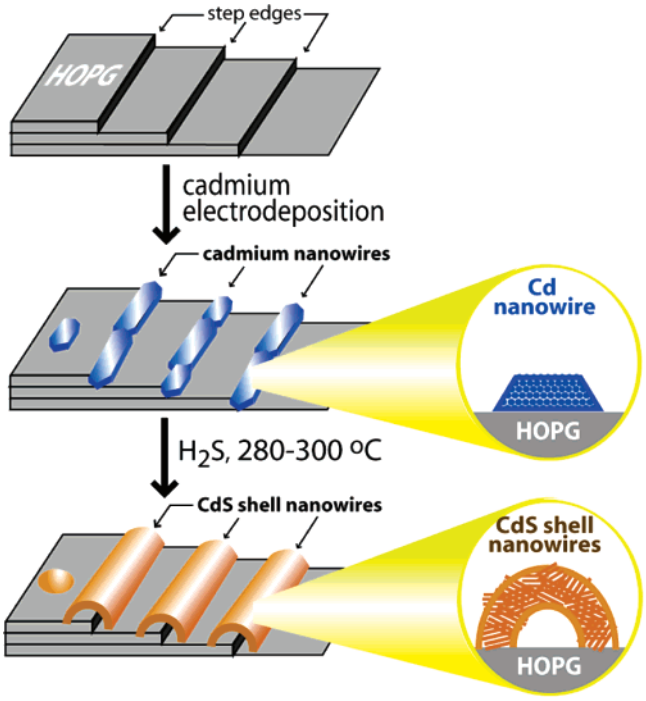

$$Cd(EDTA)^{2-} + 2e \rightarrow Cd + EDTA^{4-} \quad (1)$$

* Corresponding author. E-mail: rmpenner@uci.edu.

10.1021/nl050994x CCC: $30.25
Published on Web 08/06/2005

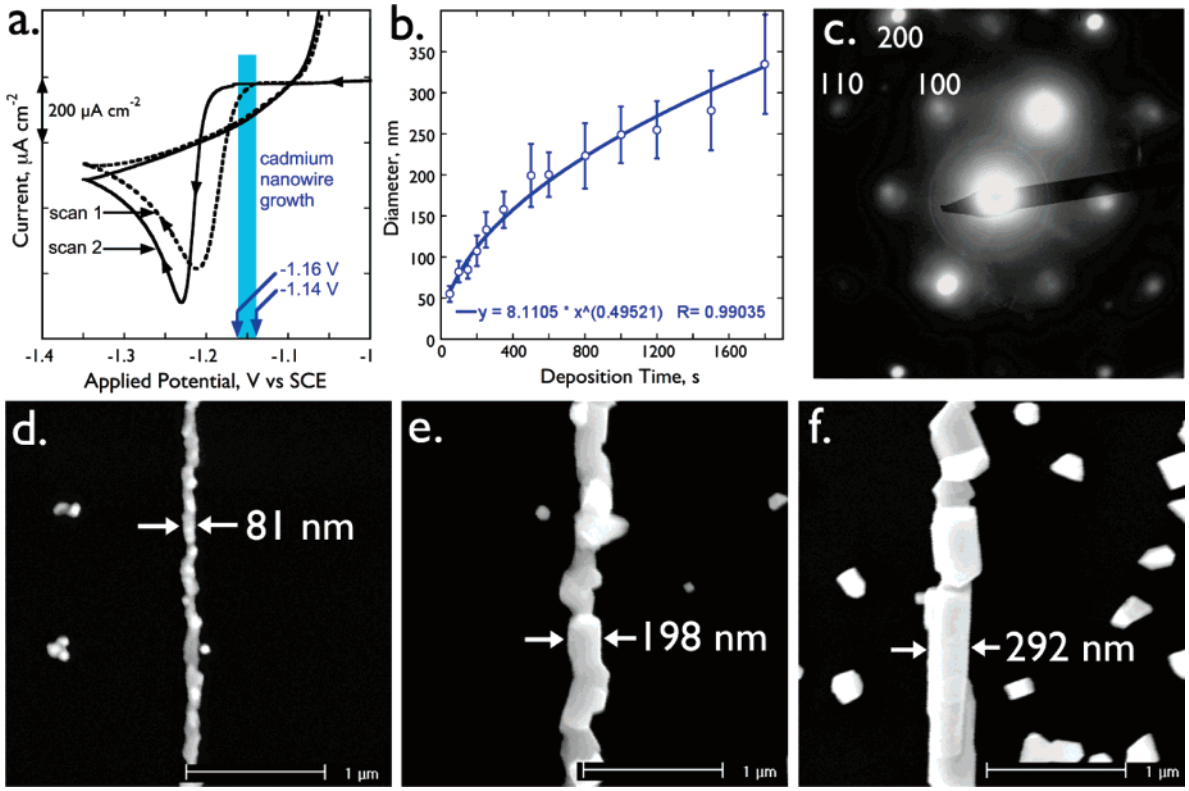

Figure 1. (a) Cyclic voltammograms at 2 mV s^{-1} for an HOPG working electrode in an aqueous plating solution containing 5 mM $CdCl_2$, 6 mM Na_2EDTA, 0.5 M NaCl, and 0.5 M NH_4Cl buffered at pH 8.5 using $NH_3 \cdot H_2O$. (b) Selected area electron diffraction pattern of a ~500 nm segment of Cd nanowire. (c) Diameter of Cd nanowires as measured by SEM plotted as a function of the deposition time. Error bars indicate $\pm 1\sigma$ in the diameter distribution. (d−f) SEMs of Cd nanowires for the electrodeposition at −1.15 V for durations of 100, 800, and 1500 s.

In the second step, Cd nanowires were converted to CdS by exposure to flowing H_2S at 280−300 °C according to the reaction

$$Cd + H_2S \rightarrow CdS + H_2 \qquad (2)$$

Cd nanowires were prepared by ESED, the selective electrodeposition of Cd at step edges on the freshly cleaved HOPG surface. Previously, ESED has been used to prepare noble metal nanowires,[20,21] metal oxide nanowires, [22,23] and nanowires composed of Bi_2Te_3.[24] Here, Cd nanowires were electrodeposited from a solution containing $Cd(EDTA)^{2-}$ because the Cd electrodeposition rate from the EDTA complex is retarded, and the step-edge selectivity is enhanced, compared to electrodeposition from a EDTA-free Cd^{2+} solution. As shown in Figure 1a, reaction 1 has an onset at −1.13 V versus SCE. Compared to a solution of Cd^{2+} in a noncomplexing electrolyte, this onset is 350 mV more negative and this is a direct indication[25] of the strong binding of Cd^{2+} by $EDTA^{4-}$ with a p*K* of 16.5. The reduction of $Cd(EDTA)^{2-}$ near this −1.13 V threshold immediately produces a Cd nucleation density at step edges of 8−12 μm^{-1}; sufficient for the formation of continuous nanowires with a minimum diameter of 50 nm. As shown in Figure 1b, the actual diameter that is obtained beyond this minimum is controllable based on the duration of the electrodeposition. Also as seen in Figure 1b, these cadmium nanowires are narrowly distributed in diameter with RSD_{dia} in the range from 13% to 19%.

Scanning electron micrographs of typical Cd nanowires are shown in Figure 1d−f. The faceted grains seen in these nanowires, particularly in Figure 1e and f, are HCP Cd single crystals as shown in the selected area electron diffraction (SAED) pattern of Figure 1c (assignable to JCPDS no. 05-0674). These SEM images reveal a surprising phenomenon: the size of single-crystalline Cd grains along the nanowire axis increases with deposition time. For the SEMs of Figure 1d−f, for example, the number density of grains along the nanowire axes increases from ~20 in Figure 1d (100 s growth time) to ~12 for Figure 1e (600 s) to ~6 for Figure 1f (1500 s). This "electrochemical annealing" is not seen with other metals we have investigated including copper, silver, gold, or palladium. A survey of many grains by SAED shows that the *c* axis of the HCP unit cell is always oriented perpendicular to the graphite surface. This high degree of orientational order may reduce the barrier associated with the coalescence and recrystallization that must be occurring to produce grain growth along the nanowire axis during nanowire growth.

As shown in Figure 2a, the increase in Cd nanowire diameter is proportional to the square root of the growth time. This proportionality is expected for the growth of hemicy-

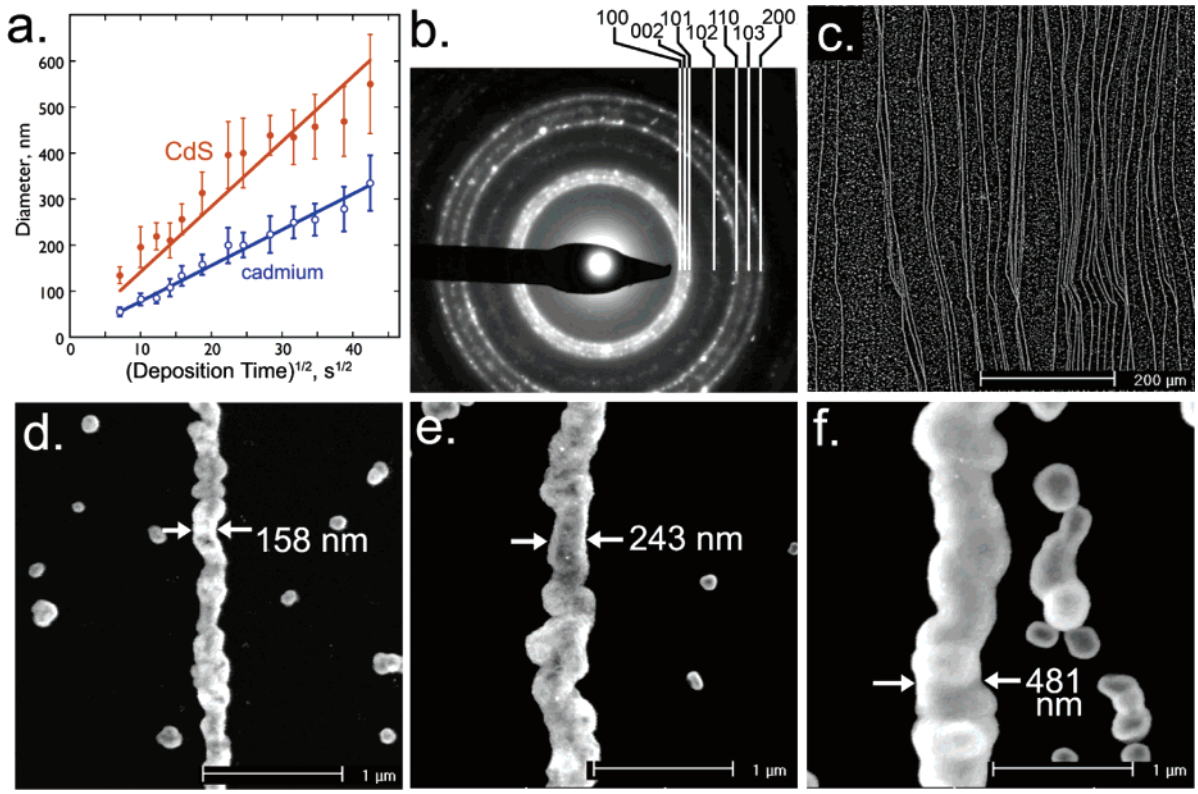

Figure 2. (a) Diameter of CdS HSNWs and Cd nanowires as measured by SEM plotted as a function of the square root of the deposition time. Error bars indicate $+1\sigma$ in the diameter distribution. (b) Selected area electron diffraction pattern of CdS HSNWs annealed in H_2S at 300 °C for 30 min. (c) Low-magnification SEM image of CdS HSNWs annealed in H_2S at 300 °C for 30 min. (d−f) SEM images of CdS HSNWs annealed at 300 °C.

lindrical wires by a constant current process, which is predicted to occur according to eq 3[18,26]

$$R(t) = \sqrt{\frac{2i_{dep}t_{dep}V_m}{\pi nFL}} \qquad (3)$$

where i_{dep} is the deposition current density, t_{dep} is the deposition duration, V_m is the molar volume of the deposited material (12.94 $cm^3\ mol^{-1}$ for Cd), n is the number of electrons transferred for the deposition of each metal atom (2 according to eq 1), F is the Faraday (96 485 C eq^{-1}), and L is the total length of nanowires per unit area on the graphite surface.

Cd nanowires were converted to CdS nanowires by exposure to flowing H_2S at 280−300 °C for 10−100 min, depending on the wire diameter. When the conversion process had proceeded to completion, SAED analyses showed continuous Debye rings of diffracted electron intensity characteristic of a polycrystalline material with a grain diameter much smaller than the sample area apertured in this measurement (dia = 2.5 μm). In the SAED pattern of Figure 2b, for example, seven diffractions can be assigned to wurtzite phase CdS (JCPDS no. 41-1049). Low magnification SEM images, like that of Figure 2c, show that these CdS nanowires retain the length and continuity of the Cd metal precursor nanowires. However, higher magnification SEM images (Figure 2d−f) reveal a dramatically changed morphology: the faceted surfaces of the Cd nanowires have been replaced by a smoothly undulating surface on the CdS nanowires.

Figure 2a shows that CdS nanowires were larger in diameter than the Cd nanowires from which they were derived by between 65% and 150%. A volume increase is expected based on the larger molar volume of CdS (29.91 $cm^3\ mol^{-1}$) compared with Cd (12.94 $cm^3\ mol^{-1}$). If the wires of both materials are hemicylindrical, then the increase in diameter expected for CdS versus Cd is calculated readily as $(29.91/12.94)^{1/3} = 1.32$, corresponding to an increase in diameter of just 32%. This means that the observed diameter increase was not caused solely by the larger molar volume of CdS. A second factor contributing to the diameter increase for CdS nanowires is apparent from high-resolution TEM images shown in Figure 3. For a Cd nanowire (Figure 3a), solid gray and black regions correspond to single crystalline grains and the uniform contrast across the width of the nanowire is in accordance with its solid nature. A TEM image of a CdS nanowire (Figure 3b), however, shows a lighter horizontal band of higher electron transparency flanked by darker edges that are nearly opaque to electrons. This electron density profile could be produced by either the nanowire structure (less CdS at the center of the wire than at the edges) or by variations in the chemical composition of the nanowire across its diameter. The lattice-resolved TEM images from the center area (Figure 3c) and the edge

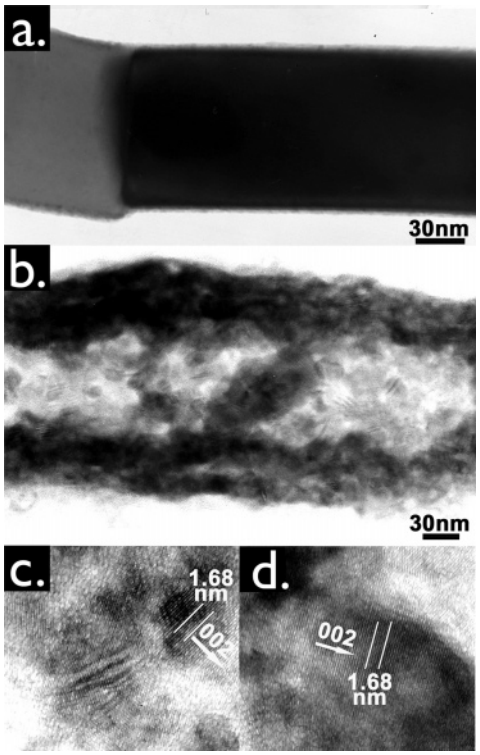

Figure 3. (a) TEM image of a Cd nanowire by electrodeposition at −1.15 V for 250 s. (b) TEM image of a CdS HSNW annealed at 300 °C for 50 min. (c) High-resolution TEM image of the center part in b. (d) High-resolution TEM image of the edge part in b.

area (Figure 3d), however, reveal the same lattice spacing of 3.36 Å, consistent with the (002) lattice spacing of wurtzite-phase CdS. So the tentative conclusion based on the TEM data is that the brightness variation across the nanowire is caused by the structure of the nanowire: specifically, electrons encounter a shorter path through CdS in the center and a longer path near the edge. Because SEM images (e.g., Figure 2d−f) clearly show that the height of the nanowire is not modulated according to this profile, the TEM images require that these CdS wires contain a hollow channel.

This hypothesis is confirmed by examining SEM images of nanowires that have been transferred to a cyanoacrylate coated glass surface (Figure 4a and b). CdS HSNWs were transferred from a conductive HOPG surface to an insulating surface using the method reported previously.[27] During the transfer operation, wires are inverted so that SEM inspection of transferred wires shows the surface of the nanowire that was in contact with the graphite surface previously. In the SEMs of Figure 4a and b, this channel is seen as a void that is surrounded by a bright shell of CdS that is in turn embedded in the darker cyanoacrylate matrix used for embedding and transfer. The formation of the CdS shell structure is caused by the Kirkendall effect.[28,29] In this case, the Kirkendall effect involves disparate rates of transport for Cd and sulfur (S) atoms through the CdS barrier layer that is formed promptly at the surface of the cadmium nanowires during conversion. CdS hemispherical shells are formed when the transport rate for Cd atoms through the CdS layer is much faster than S atom transport through the CdS layer in the opposite direction. If instead, S atom transport is faster than Cd atom transport, then conversion of the nanowire to CdS occurs at the CdS/Cd interface with the formation of a solid CdS nanowire. In the former case, involving fast Cd atom transport, cadmium is "evacuated" from the core of the nascent CdS nanowire as it undergoes conversion to CdS, just observed here. Yin and Alivisatos[30] were the first to recognize the importance of the Kirkendall effect in the formation of hollow nanometer-scale cobalt oxide and sulfide nanocrystals.

Despite the nanocrystalline nature of these nanowires, CdS HSNWs exhibited strong band-edge photoluminescence emission and photoconductivity. Photoconductivity data were acquired for ensemble CdS HSNWs that had been transferred from the conductive HOPG surface to a glass microscope slide using the method reported previously.[31] Cd HSNWs were transferred without breakage using this technique, which involves the embedding of the nanowires in a cyaoacrylate film on glass followed by lift-off of the HOPG surface. Electrical contacts were applied to the ends of nanowire ensembles by through-mask evaporation of gold; the electrically isolated nanowire length between these contacts was ∼20 μm. On the basis of SEM examination of these transferred HSNWs, we estimate that between 10 and 50 electrically continuous wires were contacted in each ensemble, but the precise number of wires contributing to conduction could not be determined. Current−voltage traces acquired in the dark (Figure 4c) were ohmic and highly resistive; for example, the particular nanowire ensemble sampled in Figure 4c had a resistance of $\sim 10^{12}$ Ω. This resistance decreased by more than 2 orders of magnitude when illuminated with an attenuated xenon arc lamp (total power = 1.4 mW, Figure 4c). The spectral response of this photoconductivity (Figure 4d) shows a sharp increase in photoconductivity as the photon energy increases from 2.25 to 2.5 eV. Between 2.5 and 2.8 eV, a plateau in the photocurrent is seen, and for higher energies up to 3.0 eV, the photoconductivity drops off slowly. The photoconductivity response onset at 2.25 eV is consistent with the known optical absorptivity of polycrystalline CdS films measured previously.[32] It is well established[33] that for conventional thin-film photoconductors, the maximum photocurrent corresponds to the wavelength at which the absorption constant is equal to the reciprocal of the sample thickness. The absorption coefficient of CdS near its absorption edge[13] is approximately 10^5 cm^{-1}, which corresponds to the sample thickness of 100 nm, in approximate agreement with the total wall thickness of the CdS HSNWs probed here.

Also shown in Figure 4d (top) is a photoluminescence (PL) spectrum for CdS HSNWs acquired at room temperature using a fluorescence microscope. CdS HSNWs within the 200-μm diameter region were excited with 150 W cm^{-2} of 257-nm light. A peak at 2.45 eV is dominant in this spectrum and is consistent with CdS band-edge emission. Not shown in Figure 4d is a broader and weaker emission centered at 1.73 eV. The emission of CdS around this region (1.6−1.8 eV) has been assigned to defect emission caused by either a Cd^{2+} vacancy[34] or by a self-activated center[35] consisting of

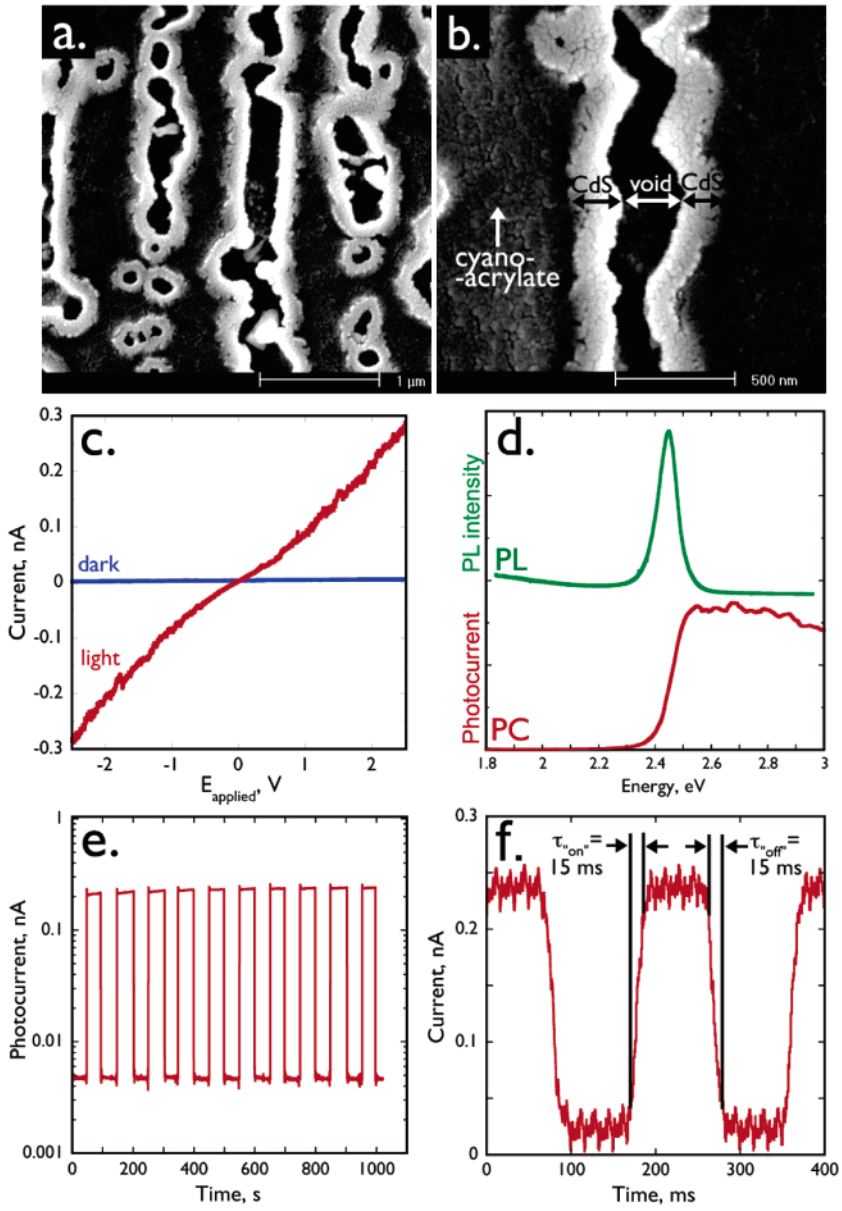

Figure 4. (a and b) SEMs of CdS HSNWs after transfer to a cyanoacrylate coated glass surface. (c) Current vs voltage curves of an array of CdS HSNWs with light on (blue) and off (red). (d) Room-temperature photoluminescence spectrum of CdS HSNWs excited at 257 nm (upper trace) and photocurrent spectrum of CdS HSNW arrays acquired using chopped, monochromatic light with a mean power of 300 μW (lower trace). Chopped excitation at 125 Hz was employed, and photocurrent was measured using a lock-in amplifier. (e and f) Reversible switching of a CdS HSNW device, biased at 2 V, between low and high conductivity states in response to chopped 300 μW excitation at 480 nm.

a Cd vacancy paired with a substitutional halogen atom. For our CdS HSNWs, the intensity of the band-edge emission was 10 times stronger than the defect emission, indicating that the defect density of the CdS SNWs is relatively small.

The photoconductivity response for CdS HSNWs can be reversible and faster than that seen in studies involving single-crystalline nanowires, as already indicated in the Introduction. The response of a typical CdS HSNW ensemble to chopped illumination (300 μW at 480 nm) is shown in Figure 4e. The "on" current and "off" current for each of the 10 cycles shown here remain the same within the noise envelope, indicating the reversibility and stability of CdS HSNWs optical switches over this time interval. The log photocurrent vertical axis here reveals that no rise time or decay of the photocurrent is observable on the time scale plotted here. A closer examination of these responses (Figure 4f) shows that they consist of flat photocurrent plateaus and are characterized by rise times and dark decay times that are both 15 ms and coincident with the instrument response time for our spectrometer. Thus, we are able to conclude only that the true photoconductivity response time is faster than ~15 ms. It is likely that the nanocrystalline morphology of these nanowires promotes a fast photoconductivity response by ensuring that photoexcited carriers rapidly recombine at grain boundaries in the dark. The hemispherical shell morphology of these wires, which exists on a much larger distance scale than the grain diameter, is unlikely to influence the photoconductivity response; however, we have

been unable to synthesize solid versions of these CdS nanowires for purposes of comparison.

It is significant, and surprising, that these CdS HSNWs simultaneously show characteristics of single-crystalline nanowires including a PL spectrum dominated by band-edge emission and a sharp photocurrent onset at the band gap. Certainly, the desirable photoconductivity properties of CdS HSNWs revealed in this study provide a strong motivation for the more thorough structural and spectroscopic investigation of these new nanomaterials.

Acknowledgment. We acknowledge the funding of this research by NSF grant DMR-0405477. We also express our appreciation to Dr. Wytze Van der Veer of the UCI Department of Chemistry Laser Spectroscopy Facility for his assistance with photoconductivity measurements, and Dr. Arthur Moore, formerly of GE Advanced Ceramics, for donating some of the HOPG used in these studies.

References

(1) Ahn, S. E.; Lee, J. S.; Kim, H.; Kim, S.; Kang, B. H.; Kim, K. H.; Kim, G. T. *Appl. Phys. Lett.* **2004**, *84*, 5022.
(2) Arnold, M. S.; Avouris, P.; Pan, Z. W.; Wang, Z. L. *J. Phys. Chem. B* **2003**, *107*, 659.
(3) Fan, Z. Y.; Chang, P. C.; Lu, J. G.; Walter, E. C.; Penner, R. M.; Lin, C. H.; Lee, H. P. *Appl. Phys. Lett.* **2004**, *85*, 6128.
(4) Heo, Y. W.; Kang, B. S.; Tien, L. C.; Norton, D. P.; Ren, F.; La Roche, J. R.; Pearton, S. J. *Appl. Phys. A* **2005**, *80*, 497.
(5) Heo, Y. W.; Tien, L. C.; Norton, D. P.; Kang, B. S.; Ren, F.; Gila, B. P.; Pearton, S. J. *Appl. Phys. Lett.* **2004**, *85*, 2002.
(6) Keem, K.; Kim, H.; Kim, G. T.; Lee, J. S.; Min, B.; Cho, K.; Sung, M. Y.; Kim, S. *Appl. Phys. Lett.* **2004**, *84*, 4376.
(7) Kind, H.; Yan, H. Q.; Messer, B.; Law, M.; Yang, P. D. *Adv. Mater.* **2002**, *14*, 158.
(8) Li, Q. H.; Gao, T.; Wang, Y. G.; Wang, T. H. *Appl. Phys. Lett.* **2005**, *86*.
(9) Liu, Z. Q.; Zhang, D. H.; Han, S.; Li, C.; Tang, T.; Jin, W.; Liu, X. L.; Lei, B.; Zhou, C. W. *Adv. Mater.* **2003**, *15*, 1754.
(10) Han, S.; Jin, W.; Zhang, D. H.; Tang, T.; Li, C.; Liu, X. L.; Liu, Z. Q.; Lei, B.; Zhou, C. W. *Chem. Phys. Lett.* **2004**, *389*, 176.
(11) Zhang, D.; Li, C.; Han, S.; Liu, X.; Tang, T.; Jin, W.; Zhou, C. *Appl. Phys. A* **2003**, *77*, 163.
(12) Gorer, S.; Ganske, J. A.; Hemminger, J. C.; Penner, R. M. *J. Am. Chem. Soc.* **1998**, *120*, 9584.
(13) Penner, R. M. *Acc. Chem. Res.* **2000**, *33*, 78.
(14) Chen, Y. T.; Ding, J. B.; Guo, Y.; Kong, L. B.; Li, H. L. *Mater. Chem. Phys.* **2003**, *77*, 734.
(15) Tang, K. B.; Qian, Y. T.; Zeng, J. H.; Yang, X. G. *Adv. Mater.* **2003**, *15*, 448.
(16) Liu, W. F.; Jin, C. G.; Jia, C.; Yao, L. Z.; Cai, W. L.; Li, X. G. *Chem. Lett.* **2004**, *33*, 228.
(17) Ip, K. M.; Wang, C. R.; Li, Q.; Hark, S. K. *Appl. Phys. Lett.* **2004**, *84*, 795.
(18) Li, Q.; Newberg, J. T.; Walter, E. C.; Hemminger, J. C.; Penner, R. M. *Nano Lett.* **2004**, *4*, 277.
(19) Li, Q.; Walter, E. C.; van der Veer, W. E.; Murray, B. J.; Newberg, J. T.; Bohannan, E. W.; Switzer, J. A.; Hemminger, J. C.; Penner, R. M. *J. Phys. Chem. B* **2005**, *109*, 3169.
(20) Walter, E. C.; Murray, B. J.; Favier, F.; Kaltenpoth, G.; Grunze, M.; Penner, R. M. *J. Phys. Chem. B* **2002**, *106*, 11407.
(21) Walter, E. C.; Zach, M. P.; Favier, F.; Murray, B. J.; Inazu, K.; Hemminger, J. C.; Penner, R. M. *ChemPhysChem* **2003**, *4*, 131.
(22) Li, Q. G.; Olson, J. B.; Penner, R. M. *Chem. Mater.* **2004**, *16*, 3402.
(23) Zach, M. P.; Ng, K. H.; Penner, R. M. *Science* **2000**, *290*, 2120.
(24) Menke, E. J.; Li, Q.; Penner, R. M. *Nano Lett.* **2004**, *4*, 2009.
(25) Bard, A. J.; Faulkner, L. R. *Electrochemical Methods: Fundamentals and Applications*, 2nd ed.; Wiley and Sons: New York, 2001.
(26) Zach, M. P.; Ng, K.; Penner, R. M. *Science* **2000**, *290*, 2120.
(27) Favier, F. W. E.; Zach, M.; Benter, T.; Penner, R. M. *Science* **2001**, *293*, 2227.
(28) Morral, J. E.; Son, Y. H.; Thompson, M. S. *Acta Metall.* **1988**, *36*, 1971.
(29) Smigelskas, A. D.; Kirkendall, E. O. *Trans. Am. Inst. Min. Metall. Eng.* **1947**, *171*, 130.
(30) Yin, Y. D.; Rioux, R. M.; Erdonmez, C. K.; Hughes, S.; Somorjai, G. A.; Alivisatos, A. P. *Science* **2004**, *304*, 711.
(31) Walter, E. C.; Favier, F.; Penner, R. M. *Anal. Chem.* **2002**, *74*, 1546.
(32) Shalimov, Kv.; Khirin, V. N.; Korolev, O. I. *Opt. Spectrosc.* **1966**, *21*, 256.
(33) Bube, R. H. *Photoelectronic Properties of Semiconductors*; Cambridge University Press: Cambridge, U.K., 1992.
(34) Berndt, R.; Gimzewski, J. K. *Phys. Rev. B* **1992**, *45*, 14095.
(35) Shiraki, Y.; Shimada, T.; Komatsub, Kf. *J. Appl. Phys.* **1974**, *45*, 3554.

NL050994X